

GT2011-46290

EXPERIMENTAL INVESTIGATION OF FORCED RESPONSE IMPELLER BLADE VIBRATION IN A CENTRIFUGAL COMPRESSOR WITH VARIABLE INLET GUIDE VANES - PART 2: FORCING FUNCTION AND FSI COMPUTATIONS

Armin Zemp*
Reza S. Abhari

LEC, Laboratory for Energy Conversion
Department of Mechanical and Process Engineering
ETH Zurich, Switzerland
e-mail: zemp@lec.mavt.ethz.ch

Matthias Schleer

ABB Turbo Systems Ltd.
Baden, Switzerland

ABSTRACT

As the second part of a two-part paper, this paper presents an experimental investigation of forced response impeller blade vibrations in a centrifugal compressor stage caused by variable inlet guide vanes. Although it is common practice to experimentally test the forced response blade vibration behavior of new impeller designs in terms of strain gauge or tip-timing measurements, the impact of the unsteady blade pressure distribution acting as an unsteady load on the blade surfaces is still not known. A centrifugal compressor impeller was therefore instrumented with dynamic strain gauges and fast-response pressure transducers to measure the forcing of the impeller blades for different compressor operating points and various inlet guide vane angle settings. The results showed a decrease in the excitation amplitudes for reduced mass flow rates of the compressor stage. The inlet guide vane angle setting affected the convection speed of the distortion pattern along the blade surface. An increase in the negative inlet guide vane angle caused higher excitation amplitudes especially in the inducer part of the blade. However, the largest negative inlet guide vane setting caused the smallest excitation amplitudes as this setup introduced the smallest amount of inlet distortion to the inlet flow field. A series of unidirectional fluid structure interaction calculations was performed to show the limitations and requirements of today's numerical tools.

NOMENCLATURE

<i>CFD</i>	computational fluid dynamics	
<i>EO</i>	engine order	
<i>FSI</i>	fluid structure interaction	
γ	inlet guide angle (relative to axial)	[°]
<i>h</i>	main blade height at leading edge	[mm]
<i>IBC</i>	inlet boundary condition	
<i>IGV</i>	inlet guide vane	
<i>Mu</i>	stage Mach number	
<i>OL</i>	operating line	
<i>p</i>	pressure	[Pa]
π_0	total pressure ratio	[—]
<i>Q</i>	corrected mass flow rate	[—]
\dot{V}	volumetric flow rate	[m ³ /s]
<i>VIGV</i>	variable inlet guide vane	

Sub-, Superscripts:

<i>PS, SS</i>	blade pressure side, suction side
<i>ref</i>	reference quantity
<i>()'</i>	fluctuation

*Address all correspondence to this author.

INTRODUCTION

In turbomachinery rotating components are subject to vibration. In particular this applies to rotating blades, which are one of the main contributors to operational failures, as identified by *Srinivasan* [1]. A potential source of forced response blade vibrations is the unsteady fluid structure interaction as conditioned in the inlet section of a centrifugal compressor from duct bends, struts or inlet guide vanes.

It is common practice to experimentally test the forced response blade vibration behavior of new impeller designs in terms of strain gauge or tip-timing measurements. The goal of both approaches is to quantify the vibratory stress levels and to decide whether they are within a tolerable range to guarantee the mechanical integrity of the components. However, the unsteady blade pressures acting as an unsteady load on the blade surfaces are still not known. With today's computational tools to calculate the time-resolved flow field, designers can perform a number of flow simulations which facilitate a parametric study and cross-comparison of the numerical predictions. However, there is still a lack of experimental data to validate the calculated unsteady blade pressure distributions from numerical simulations. Furthermore, numerical prediction of the unsteady blade pressure fluctuations are sensitive to a number of factors, such as boundary conditions, blade boundary layers, clearance flows, operating point, etc. which might significantly influence the calculated unsteady excitation forces. Therefore, the resultant excitation of the blades can only be captured by the direct measurement of the unsteady pressures on the blade surfaces in an experimental investigation under engine representative conditions.

Steady and unsteady blade pressure measurements were presented by *O'Brien et al.* [2], *Lakshminarayana* [3] and *Chivers* [4]. In a series of publications, blade pressure measurements were reported for short-duration test turbines by *Dunn et al.* [5] and *Dunn* [6]. A comparison with computational prediction was performed by *Dunn et al.* [7] and *Rao et al.* [8]. Their work focused on capturing the effects of blade row interaction in the flow field. The importance of blade pressure distribution and its measurement in experimental heat flux research and computational predictions was also presented in great detail by *Dunn* [9]. Unsteady pressure measurements in a short-duration test facility were performed by *Miller et al.* [10, 11] in order to identify blade row interaction mechanisms and to quantify their effect on the unsteady blade surface pressure distribution. Experimental research of a similar nature was carried out by *Dénos et al.* [12, 13] for a transonic turbine stage. Blade surface pressure was measured to capture the complex blade row interactive flow phenomena and the results were compared to a three-dimensional flow computation. Investigations in the field of unsteady blade surface pressure

measurements and forced response were carried out for an axial flow research compressor by *Manwaring and Fleeter* [14, 15] and *Rabe et al.* [16]. Their work showed the impact of inlet flow distortion and wake-generated flow non-uniformities on the unsteady forcing function. The effect of asymmetric aerodynamic perturbations on the forced response of bladed disks was presented by *Miyakozawa et al.* [17]. A recent publication by *Kammerer and Abhari* [18] presented blade pressure measurements in a high-speed centrifugal compressor stage. In this work the flow upstream of the impeller was intentionally disturbed using distortion screens. The resultant unsteady pressures caused resonant blade vibrations.

Parallel to the experimental work, the time-resolved computation of the flow and the structure can be performed to calculate the stress distribution within the structure. Two different approaches can be used. Firstly, the fluid and solid domains can be fully coupled to calculate the bidirectional fluid structure interactions and secondly, the fluid and solid domains can be handled as decoupled systems to perform a unidirectional fluid structure interaction calculation. In the latter case the overall damping ratio is required as an input for the forced response *FEM* model and has to be experimentally estimated. The unsteady pressure distribution acting as an unsteady load on the blade surfaces needs to be provided by 3D unsteady *CFD* calculations. *Filsinger et al.* [19, 20] proposed an approach for a decoupled *CFD – FEM* analysis and discussed the results for a series of unidirectional *FSI* calculations for an axial turbocharger turbine. *Dickmann et al.* [21] presented a unidirectional fluid structure interaction calculation for centrifugal compressor forced response blade vibrations caused by a non-uniform inlet flow field.

MOTIVATION AND SCOPE OF THE PAPER

This work was motivated by the need for reliable and engine representative data to advance the understanding of forced response blade vibrations of centrifugal impeller blades in a radial compressor with variable inlet guide vanes to develop and validate numerical tools used during the design process. This paper aims to present and discuss unsteady blade pressure measurements from an experimental investigation on forced response blade vibrations in a centrifugal compressor with variable inlet guide vanes. In the first part of this paper the influence of the inlet guide vane angle setting and the operating point on the forcing function will be detailed. The measurements of the distorted inlet flow field presented in Part 1 [22] of this two-part paper were used as inlet boundary conditions for a series of 3D unsteady *CFD* simulations. The calculated amplitudes and phase angles of the unsteady loads were compared to the measured values. In the second part of this paper the predicted time-resolved blade pressures were then used as input for a unidirectional *FSI* calculation. The required overall damping ratios for the calculations

were estimated in Part 1. The predicted stress levels from the forced response *FEM* calculation were compared to the measured levels in the experiments. Not only the requirements, but also the limitations of the numerical approach used to predict the vibratory stress levels will be discussed.

TEST FACILITY AND EXPERIMENTAL APPROACH

Test Facility

The experimental investigation was performed in the 'RIGI' single-stage centrifugal compressor rig at the Laboratory for Energy Conversion at the Swiss Federal Institute of Technology in Zurich, Switzerland.

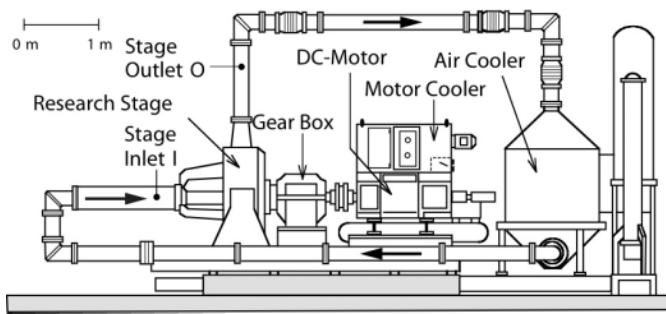


FIGURE 1. Centrifugal Compressor Test Facility

The rig is operated in a closed loop arrangement which facilitates control of the inlet pressure and temperature independent of ambient conditions. The impeller is driven by a 440 kW DC motor with a two-stage gearbox and the maximum shaft speed is limited to 22'000 rpm. The impeller in use for the present investigation has an outer diameter of 400 mm and features 7 main and 7 splitter blades. Downstream of the impeller the rig is equipped with a parallel-wall vaneless diffuser with an exit diameter of 580 mm and a diffuser channel height of 15.8 mm. The design total pressure ratio is $\pi_0 = 2.8$ at a design volumetric flow rate of $\dot{V} = 3.5 \text{ m}^3/\text{s}$. A detailed description of the impeller design is given by *Schleer* [23]. Downstream of the compression stage, the working fluid is cooled by a heat exchanger and discharged with a throttle device. The throttle is also used to set the requested mass flow rate. The mass flow is measured with a standard orifice downstream of the throttle. The performance of the compressor is estimated by the measurement of temperatures and pressures upstream and downstream of the compression stage. Figure 1 shows a schematic drawing of the test facility.

Variable Inlet Guide Vanes in Centrifugal Compressors

Centrifugal compressors in industrial applications are operated over a wide range of mass flow rates at constant

pressure ratios with constant rotational speeds. The use of variable inlet guide vanes (*VIGV*) in a centrifugal compressor permits adjustment of the rotor inflow properties and also facilitates a reduction in the power required to start up the compressor.

The integration of inlet guide vanes upstream of the centrifugal compressor impeller introduces flow distortions. These non-uniformities in the inlet flow field may interact with the impeller blades and therefore are a possible source of forced response blade vibrations.

Experimental Setup

Figure 2 shows the experimental setup in the inlet section of the test rig. The main components of the setup are the inlet guide vanes, the rotary transmitter, the access for aerodynamic probe measurements downstream of the *IGV* row and the impeller instrumented with blade-mounted dynamic strain gauges and fast-response pressure sensors. The *VIGV*s are 2.5 impeller blade heights upstream of the impeller eye. The aerodynamic probe measurement plane is 1 blade height h downstream of the *VIGV* row and 1.5 blade heights upstream of the impeller eye. The rotary transmitter in the center of the suction pipe was required to transfer the signals from the dynamic strain gauges and pressure transducers mounted on the blade surfaces to the data acquisition system.

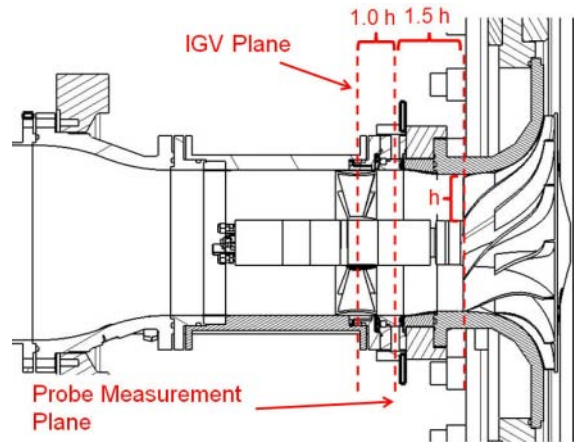


FIGURE 2. Experimental Setup within Suction Pipe

Flow Field Measurement Downstream of the IGV

A miniature pneumatic four-hole probe was used to measure the 3D steady flow properties downstream of the inlet guide vanes. The cylindrical probe has a calibration range of $\pm 30^\circ$ in yaw and $\pm 24^\circ$ in pitch angles. The probe tip diameter is

1.8 mm. A detailed summary of the probe properties was given by *Lenherr et al.* [24]. The probe was mounted on a traversing system, which enabled the automatic positioning of the probe head in radial as well as in circumferential directions. The measurements of the distorted flow field downstream of the *IGV* row were crucial to quantify the amount of non-uniformity introduced into the flow and to visualize the distortion pattern within the flow. The measured flow properties were used as inlet boundary conditions for the 3D unsteady *CFD* calculations to assess the unsteady impeller blade pressure distribution for a set of different operating points. The results from the probe measurements of the distorted inlet flow field are presented in Part 1.

On-Blade Pressure and Strain Measurements

On-blade pressure and strain measurements on rotating impeller blades impose a number of requirements on the sensor application and design. The sensors must be able to endure the harsh environment, but must also exhibit sufficient sensitivity to acquire the strain and pressure fluctuations. *Kammerer and Abhari* [18] presented an experimental set-up that allowed them to measure the strain levels and pressure fluctuations on the blade surface of a high-speed centrifugal compressor impeller. The strain gauges are located close to the shroud line on the blade suction side as shown in figure 4. This location was chosen to allow measurement of a variety of resonance modes with the same strain gauge position. As the sensor is therefore not placed at the position of highest strain for each resonance mode, transmission factors are calculated to correlate the measured strain and the maximum stress. The design of a new pressure sensor was realized based on previous in-house work undertaken in the field of fast aerodynamic probes. The design of the pressure sensors was based on the developments presented by *Gossweiler* [25], *Kupferschmied* [26] and *Pfau et al.* [27]. The final design of the pressure sensor consisted of a piezo-resistive silicon-based die packaged into a carrier and connected to a flexible connector. The die was fixed and sealed using silicon, such that it functions as an absolute pressure sensor and is covered by a thin layer of silicon which acts as a protective layer. The packaging technique made a miniaturization of the sensor down to $1.1 \times 0.35 \times 3$ mm possible. The primary need for the miniaturization was the requirement to install the sensors on impeller blades with a thickness of only a few millimeters. The pressure sensors were flush-mounted into the pockets and the flexible connectors were glued onto the blade surface.

A total of 16 pressure sensors were installed in pairs with eight sensors on each blade side. Figure 3 illustrates the sensor distribution in the meridional view. The sensor distribution shown was chosen in order to allow for measurements of the forcing function that excites the blades within the inducer part. On the circumference the sensors had to be distributed

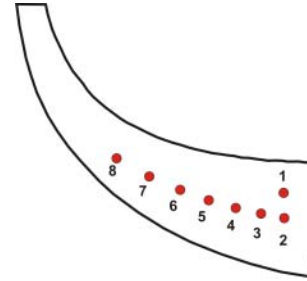


FIGURE 3. Pressor Sensor Location on the Impeller Main Blade

among all blades. This was necessary in order to reduce the risk of potential blade damage during operation resulting from excessive stress concentration introduced by the notch effect of the pockets machined into the material. Figure 4 shows a photograph of the instrumented impeller. In addition to the pressure sensors, each main blade was equally equipped with one strain gauge to acquire the vibratory response levels of the blades. A detailed description of the transient measurement approach and the damping estimation procedure from dynamic strain gauge measurements is given in Part 1 of this two-part paper.

The frequency bandwidth of the applied pressure sensors was obtained from shock tube experiments. The response to the step excitation on the pressure sensor was measured and the results showed a response at 42 kHz corresponding to the first eigenfrequency of the sensor assembly. This was assumed to give a considerable margin with respect to the maximum frequencies intended to capture during measurements which are in the order of 5 kHz.

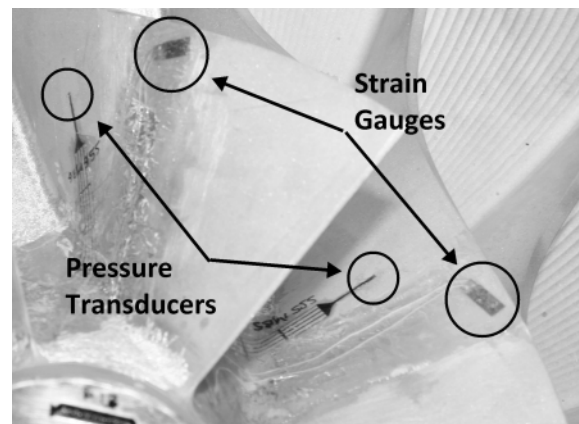


FIGURE 4. Instrumented Centrifugal Compressor Impeller

As the blade vibrates, mechanical strain can be transmitted into the pressure sensitive die and could be interpreted as a change in the measured pressure. Kammerer [28] showed that strain-induced effects were insignificant during off-resonant signal acquisition, but this was not the case for pressure measurements during resonance, where the contribution from deformation effects might amount to as much as 10% of the overall pressure signal.

Due to the closed loop arrangement of the test rig the pressure signal calibration was performed within the facility prior to each run. The pressure within the facility was changed within a range of 0.2 bar to 0.9 bar, which corresponded to the intended operating regime during rotational operation. To relate pressure and sensor behavior a linear relation was used, where the unknown gains and offsets had to be calibrated. In the present application gain varied on average by 5%. This effect was systematic and could be accounted for for each sensor individually, thereby reducing the influence on the uncertainty. In practice this was done by monitoring the inlet pressure upstream of the impeller during measurements, which was then used to adjust the gain to the appropriate level. For off-resonance conditions the overall uncertainty was estimated to be $\pm 5\%$ of the measured pressure level and for measurements during resonance the overall uncertainty increased to $\pm 11\%$ caused by the influence of the blade deformation on the sensor output signal.

CFD Model and Simulation Setup

The computational domain for the 3D unsteady *CFD* calculations corresponded to the experiment, as seen in figure 2, with the inlet of the domain at the location where the probe measurements were performed and the with the outlet of the numerical model at the diffuser exit. The computations were performed with the commercial *ANSYS CFX V12.1* software package. The grid for the unsteady computations represented the entire impeller due to the different spatial extent of the distortion pattern over the seven main blade pitches and consisted of 6.5×10^6 nodes that made up 5.9×10^6 hexahedral elements. One revolution of the impeller was divided into 2^7 time steps. This yielded a 2.81° turn of the impeller for each time step which was considered to be sufficient to resolve the inlet distortion pattern and its convection through the compressor stage. The *k-ε* turbulence model with scalable wall functions was used in the unsteady *CFD* simulations. For the spatial discretization as well as for the assessment of the periodic convergence the approach and settings presented by Zemp *et al.* [29] were used. The measured total pressures, total temperatures and flow angles from probe measurements were used as inlet boundary conditions for the time-resolved calculations. At the outlet of the domain the average static pressure over the entire outlet area was adjusted such that the computed mass flow could be matched to the measured mass flow in the experiment.

Resonance Blade Analysis and FSI Calculation

To determine the dynamic behavior of the tuned compressor impeller a cyclic symmetric finite element model including the main blade, the splitter-blade and the hub sector was built with parabolic brick and wedge elements. Prior to the dynamic analysis of the eigenfrequency the static load due to rotation was applied. The static and vibration analysis of the rotating impeller were performed using the commercial *ABAQUS FE* software. The stress distribution for the first main blade resonance is plotted in figure 5. A comparison of the measured resonance frequency and the calculated eigenfrequency showed a difference between the calculations of 4%, which is well within normal experience for this kind of resonance.

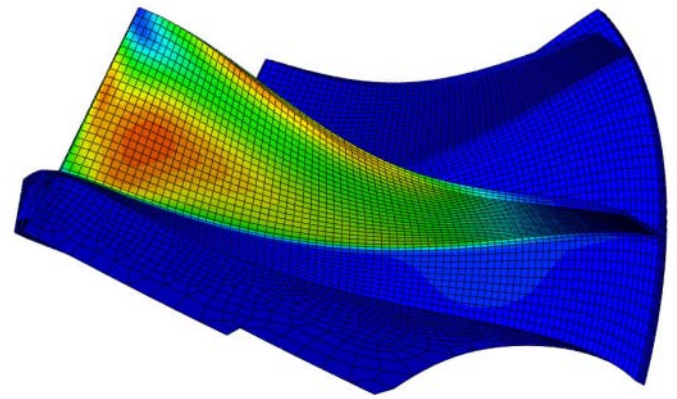


FIGURE 5. Normalized Stress Distribution for Main Blade Mode 1

Based on this calculation the transmission factor for correlating the measured strain and the maximum stress within the first main blade resonance was evaluated. For the given strain gauge placement a transmission factor of 63% Youngs Modulus was computed.

A pressure distribution on the blade surface was obtained out of the unsteady *CFD* calculation for each time step. This pressure information was decomposed into the Fourier space and provided the exciting pressure load (containing phase and magnitude information) for each excitation order. As the discretization of the *CFD* and the *FE* model was not consistent, a mapping algorithm was applied to transfer the exciting pressure in the Fourier space onto the forced response calculation mesh.

To set up the uni-directional fluid structure interaction calculation the pressure distribution in the investigated excitation order was applied to the cyclic symmetric finite element model and a forced response analysis was performed. For the spatial extrapolation of the *CFD* data onto the contour of the cyclic *FE*

mesh of one sector of the radial impeller, the in-house design tool of ABB Turbo Systems Ltd. was used. For the association of points of the *CFD* mesh with single element faces on the *FE* contour, a weight function is defined using the distance tolerance based on the characteristic element size of the blade and hub contour. The procedure results in weighted *CFD* static and excitation amplitudes, which are associated with the appropriate element face of the *FE* mesh. The *CFD-FE* interaction process was presented in detail by *Schmitz et al.* [30] and *Dickmann et al.* [21,31]. The forced response calculations delivered the blade stress in resonance condition with the excitation for each forcing function given by the unsteady *CFD* calculation.

RESULTS

In the following sections results are presented for experimental and numerical investigations at different compressor operating points and for varied inlet guide vane angle settings. The parameters were independently investigated to separate out the effects on the unsteady blade forcing. Results for three different *IGV* angles γ (0° , -30° and -45°) are presented. The negative angle indicates a pre-swirl in a counter direction to impeller rotation. The effect of the pre-swirl on the compressor performance and the results from probe measurements of the distorted inlet flow field downstream of the *IGV* row are shown in Part 1 of this two-part paper. The results presented focus on the resonant response of the centrifugal impeller main blade for blade mode 1 excited by its fundamental frequency at *EO12* caused by the 12 inlet guide vanes. The measured Campbell diagram is shown in figure 7.

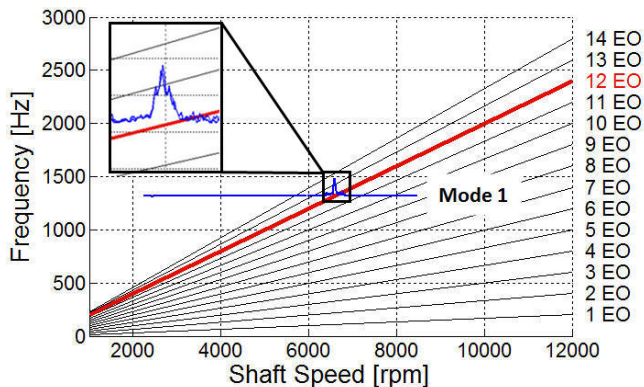


FIGURE 7. Campbell Diagram for the Impeller Main Blade

As the impeller blades passed through the resonant response the blade deflection caused a superimposed pressure field in addition

to the unsteady pressure caused by the inlet guide vanes. The sensor output was also influenced by mechanical strain transmitted into the pressure sensitive die, as the blade vibrates. The resultant pressure was measured by the blade-mounted pressure transducers. Figure 6(a) shows the evolution of the unsteady blade pressure for a transient measurement with constant shaft speed sweep rate for the pressure sensor at location 1 (see figure 3) and the corresponding strain gauge response in figure 6(b). As the resonant blade vibration occurred the pressure sensor signal clearly represented the influence of the blade deflection on the pressure sensor output. Above and below the resonant shaft speed the sensor showed the forcing function in terms of unsteady blade pressures. The unsteady blade pressure distributions are compared for off-resonance conditions in order to exclude the contamination of the pressure sensor output by resonant blade vibration.

For this paper experiments were performed for three different throttle settings. The resulting operating lines are illustrated on the compressor map in figure 8. *OL1* corresponds to a near-choke condition, *OL2* to a realistic setting during operation and *OL3* to a near-stall operating condition for the centrifugal compressor rig.

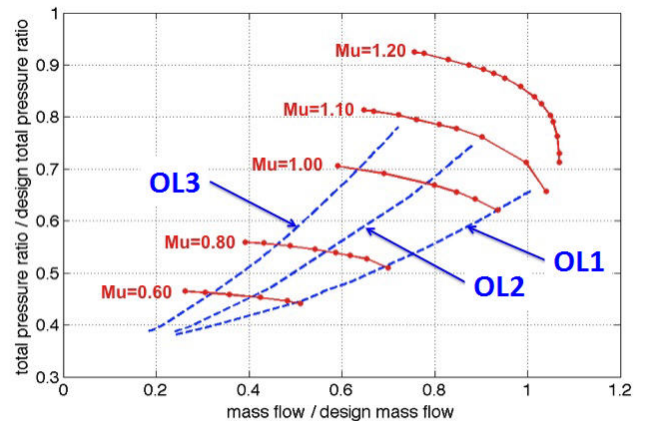


FIGURE 8. Compressor Map and Operating Lines

Forcing Function – Amplitude and Phase Angle

In the following the pressure distributions along blade mid-span from leading to trailing edge of the main blade for one impeller revolution are compared for varied *IGV* angle settings and different compressor operating points. The measured un-

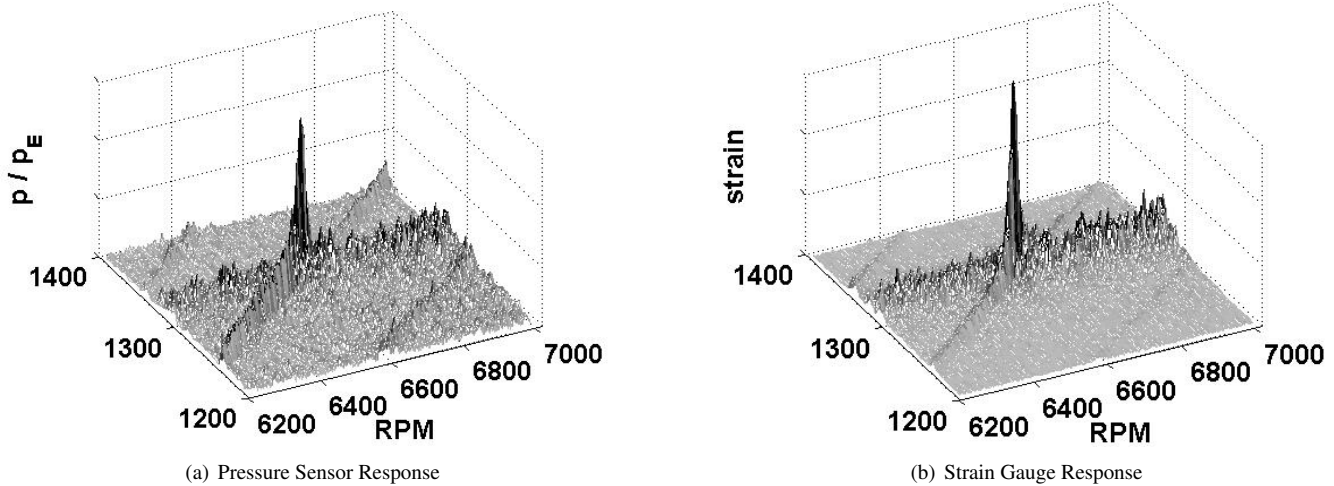


FIGURE 6. Typical Strain Gauge and Pressure Sensor Signal during Resonant Response

steady pressure fields on the main blade surfaces are compared to calculated blade pressure distributions from unsteady *CFD* simulations. To exemplify figure 9 shows a measured unsteady pressure distribution for the 0° *IGV* angle at 0.8 bar inlet pressure for *OL2*. The plotted range from the leading to the trailing edge of the main blade corresponds to the locations of sensors 2 to 8 (Figure 3). The unsteady pressure load remained almost constant within the covered meridional length and the *EO12* excitation over one impeller revolution could clearly be identified.

The superimposed subharmonic *EO2* excitation was identified as a relic from the cooling lines of the rotary transmitter. The two tubes for coolant supply and return cross the suction pipe five blade leading edge heights h upstream of the impeller eye in opposite directions. The amount of flow distortion introduced to the inlet flow field is strong enough to impact on the main blade surface.

To simplify the comparison between different operating points, the amplitudes and the phase angles of the fundamental excitation along the meridional length of the blade at 50% blade span were extracted from the time-space diagrams. This enabled an explicit comparison of the measurements for different *IGV* angles and compressor operating points.

To detail the effect of the throttle setting on the unsteady blade pressure acting on the blade surface, the amplitudes and phase angles for *OL1* at near-choke, *OL2* at a design throttle setting and for *OL3* (near-stall) were extracted from the measurements with the -30° *IGV* angle setting. The comparison in figure 10(a) showed the highest amplitudes along the blade for the

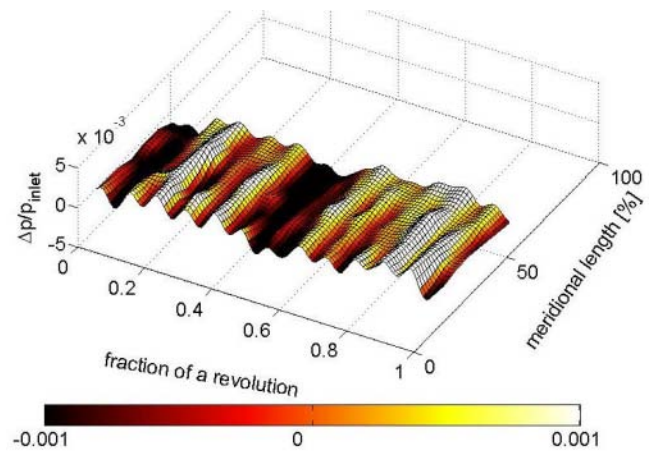


FIGURE 9. Measured Unsteady Blade Pressure Fluctuation $\Delta p'_{PS-SS}$ at Mid-Span, 0° *IGV* at *OL2*

near-choke operating line, except for the sensors in the inducer part at 10% meridional length. For all three cases, the curves showed an increase in the $\Delta p'$ from 40% towards 50% meridional length. The unsteady pressure loads for *OL2* and *OL3* were in a comparable range. However, as the corrected mass flow was reduced from *OL1* to *OL2* and *OL3*, the amplitudes showed a tendency to increase towards the leading edge of the blade. Although the amplitudes increased for lower mass flow ratios, the strain measurements discussed in Part 1 of this two-part paper showed the highest response levels for *OL1*. Therefore, as the phase angles in figure 10(b) did not show a significant difference for the three throttle settings, the increased unsteady blade pressure from 20% to 50% meridional length for the near-choke oper-

ating point was assumed to be the reason for the highest resonant response levels measured with the strain gauges. The excitation amplitude in this region was about two times higher for the *OL1* case compared to the two others. The continuous decrease of the phase angles represents the downstream convection of the pressure distortion pattern along the blade surfaces.

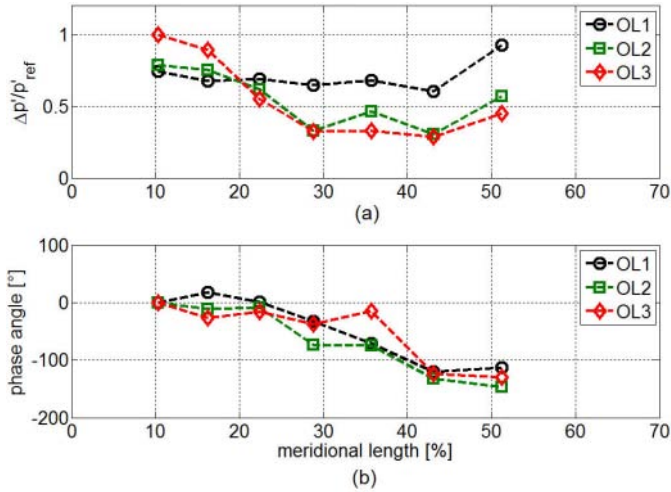


FIGURE 10. Measured Amplitudes and Phase Angles of the Unsteady Blade Pressures, -30° IGV Angle at *OL1*, *OL2* and *OL3*

The influence of the *IGV* angle setting on the amplitudes and phase angles is illustrated in figure 12 for *OL2*. The evolution of the amplitude for the -30° case has already been discussed. The unsteady blade pressure for the 0° angle was found to be almost constant along the blade. The lowest excitation forces could be found for the -45° *IGV* setting, except for a peak amplitude in the inducer section.

The reason for the lowest unsteady pressure load is represented in figure 11, where the aerodynamic probe measurements downstream of the inlet guide vane row showed reduced relative flow field distortions for the -45° compared to the -30° case. The decreased amount of inlet distortion was caused by enhanced mixing and an increased flow path length for the swirling flow from the *IGV* plane to the impeller eye. In the tip region and down to about 50% blade span the low momentum wake regions caused by the inlet guide vanes had already completely mixed out.

The corresponding phase angles in figure 12(b) showed the higher convection speed of the distortion pattern along the blade surface in the case of the -30° guide vane angle compared to

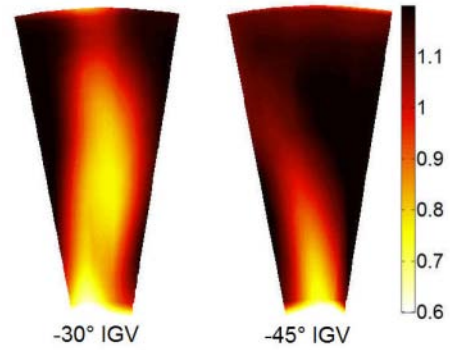


FIGURE 11. Measured Normalized Absolute Mach Number at $Q/Q_{des} = 0.48$, 1.5 Blade Heights Upstream of the Impeller

the 0° setting. This is caused by the increased corrected mass flow for larger negative inlet guide vane angles at a constant shaft speed. However, the -45° case did not follow this trend as the shape of the blade wakes changed completely.

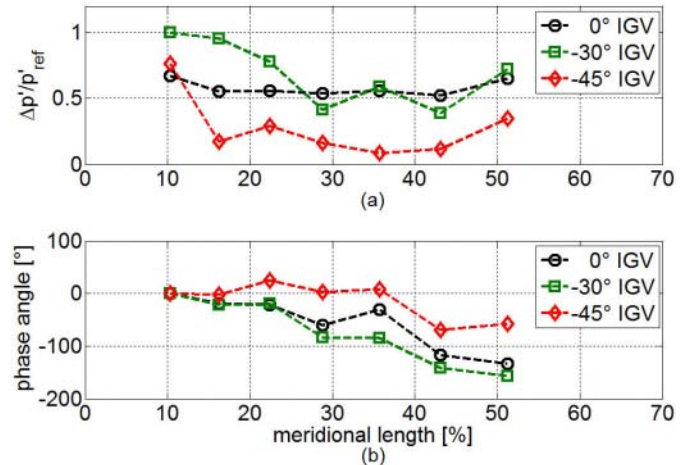


FIGURE 12. Measured Amplitudes and Phase Angles of the Unsteady Blade Pressures (0° , -30° and -45° IGV Angle) at *OL2*

A series of 3D unsteady *CFD* simulations were performed to calculate the time-resolved blade surface pressure distributions at the same compressor operating points as in the experiments. The comparison of the results from *CFD* simulations with the experiments for different *IGV* angles and compressor operating points permitted the validation of the numerical predictions which were used as an input for the set of forced response *FEM* calculations presented in the second part of the results section.

The validation of the numerical predictions was done based on a comparison with measured blade pressures in the experiments. Figure 13(a) shows the measured and computed amplitudes for the -30° IGV setting at OL3. Overall, the calculated amplitudes matched the measured values. In contrast to the experiment, the CFD simulation showed a higher unsteady pressure load from 25% to 50% meridional length. The phase angle of the excitation is shown in figure 13(b). Although the two curves evolve differently between 10% and 45% meridional length, the mean convection speed of the distortion pattern along the blade surface in the simulation was similar to the measured phase angle in the experiment.

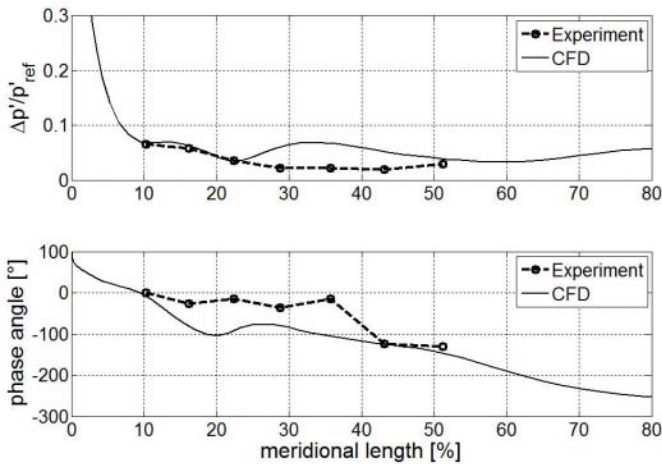


FIGURE 13. Comparison of Measured and Computed $\Delta p'_{PS-SS}$, -30° IGV, OL3

The comparison was performed for all the unsteady CFD simulation results used as input data for the forced response FEM calculations presented in this paper. The deviations from the CFD calculations compared to the measurements were of the same order of magnitude as for the case presented here. Overall, the differences between the predictions and measurements were assumed to be small enough to justify the use of the CFD approach to provide valid predictions of the time-resolved flow field.

To detail the influence of the inlet boundary condition of the distorted inlet flow field downstream of the IGV row on the predicted unsteady blade pressure distributions one simulation was performed where the inlet guide vane row was part of the CFD model. The calculated excitation amplitude and phase angle were compared to the calculation with the measured flow properties at the CFD domain inlet and to the measured values in the experiment. For the numerical model containing the inlet guide vanes,

the total pressure and total temperature distribution of the suction pipe upstream of the guide vanes were applied as inlet boundary conditions. The comparison was performed for the -30° IGV setting at OL2 and the results are shown in figure 14. Although the phase angles for the three curves coincide along the blade, the unsteady pressure load was significantly underestimated in the CFD simulation that included the inlet guide vanes, especially in the inducer section of the blade.

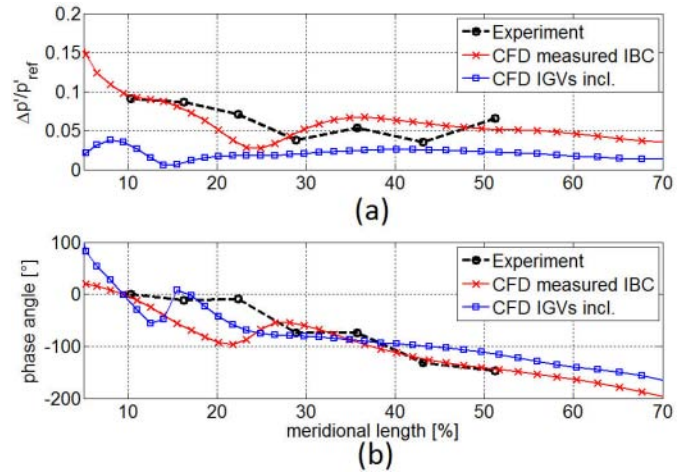


FIGURE 14. Influence of Inlet Boundary Condition on Calculated $\Delta p'_{PS-SS}$, -30° IGV, OL2

The effect of this underestimated unsteady pressure load on the blade stress distribution calculated with the forced response FEM model will be detailed in the following section.

Calculated Blade Stress Distribution and Comparison with Experiment

Using the aerodynamic probe measurements of the distorted inlet flow field downstream of the inlet guide vane row as inlet boundary conditions for the unsteady CFD prediction of the time-resolved blade pressure distributions and the blade damping properties from dynamic strain gauge measurements as input data for the FSI model, the in-house design tool of ABB Turbo Systems Ltd. was used to calculate the vibratory stress levels within the impeller blades during resonant response. The calculated stress distribution within the blade was compared with the dynamic strain gauge measurements presented in the Part 1 paper. The comparison was performed for the 0° and the -30° IGV angles. Figure 15 shows the calculated and measured stress levels at OL1, OL2 and OL3 for the 0° configuration. The error bars for the measured stress levels show the difference between

the seven impeller main blades. The trend to lower stress levels at lower mass flow rates from *OL1* to *OL3* was reproduced by the *FSI* calculations. However, for the specific cases presented in this paper there is an offset between the experiments and the numerical predictions for all three compressor operating points. The calculation showed lower stress levels and under-predicted the values by about a factor of 3 to 4.

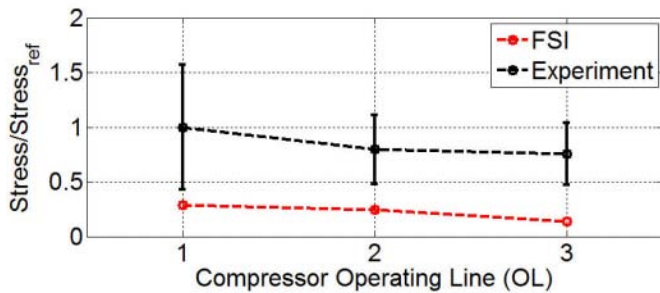


FIGURE 15. Measured and Calculated Blade Stresses Normalized by Maximum in Experiment, 0° IGV Angle

The comparison for the -30° case in figure 16 shows an over-prediction of the calculated stress level at *OL2* by a factor of about 2. This was the only case where the *FSI* calculation resulted in higher stress levels compared to the experiment, although the validation of the calculated blade pressure distribution in terms of amplitude and phase angle in figure 14 showed a reasonable match with the experimental values. The calculations showed lower values for *OL1* and *OL3*, but the difference between the numerical prediction and the experimental values was smaller than for the 0° IGV setting. The stress levels from the *FSI* calculation were about 10% to 25% lower than the values from the experiments. Therefore a simple correction for the offset in the calculated values can not be applied.

The influence of the compressor operating point on the blade stress levels was stronger in the case of the -30° IGV angle compared to the 0° case and the blade to blade variation in the experiment decreased at higher negative inlet guide vane angles.

To demonstrate the importance of the inlet boundary condition on the subsequent numerical prediction of the stress levels in the impeller blades the unsteady blade pressure distribution was calculated with a *CFD* model that contained the *IGV* row. Upstream of the inlet guide vanes, the total pressure and temperature distributions within the suction pipe were applied as inlet boundary conditions for the simulation. The resulting pressure fields were used as an input for the forced response calculation.

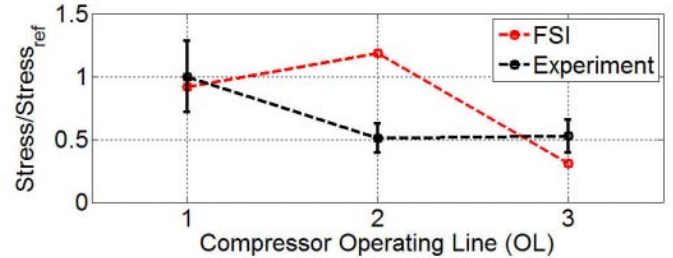


FIGURE 16. Measured and Calculated Blade Stresses Normalized by Maximum in Experiment, -30° IGV Angle

The comparison showed a significant under-prediction of the stress level in the impeller blade. The calculated stress level is more than one order of magnitude lower than the measured value.

The reliable prediction of the stress levels without the measured flow field downstream of the inlet guide vane row used as an inlet boundary condition for the time-resolved *CFD* calculation was not possible for the specific configurations presented in this paper. Although the fluid mesh in the suction pipe upstream of the impeller eye and in the *IGV* section was assumed to be fine enough, the inlet flow distortion caused by the inlet guide vanes was not translated properly onto the impeller main blade surfaces.

SUMMARY AND DISCUSSION

Unsteady blade pressure and dynamic strain gauge measurements were performed for forced response impeller blade vibrations in a centrifugal compressor stage with variable inlet guide vanes. Experiments were performed for three different compressor operating points and inlet guide vane angle settings. Generally, the amplitude of the blade forcing decreased for lower mass flow rates. The comparison of the amplitude and phase angle of the unsteady blade pressure distribution acting as an unsteady load on the main blade surfaces for three different inlet guide vane angle settings (0° , -30° and -45°) showed an increased excitation amplitude in the inducer part of the blade for the -30° case compared to the 0° setting. However, the -45° IGV setting showed the lowest amplitudes, caused by a reduced amount of flow non-uniformity translated from the inlet guide vanes onto the impeller blade surfaces. The phase angles for the three cases clearly represented the higher convection speed of the distortion pattern along the blade surfaces in the case of an increased amount of pre-swirl.

The measured unsteady blade pressure distributions were used to validate the predicted excitation amplitudes from a series of 3D unsteady *CFD* calculations. Overall, the difference in

terms of amplitudes and phase angles of the unsteady blade pressure distributions between numerical predictions and the experiments was assumed to be small enough to justify the use of the flow calculations to provide valid predictions of the time-resolved flow field.

A series of forced response calculations was performed with an industry design tool to predict the stress distribution within the impeller blade. The predicted unsteady blade pressure distributions from unsteady *CFD* calculations, with the measured flow fields downstream of the inlet guide vane row applied as inlet boundary conditions, and the experimentally estimated blade damping properties were used as inputs for *FSI* calculations. Generally, for the specific case presented in this paper the *FSI* calculation under-predicted the stress levels by a factor of about 3 to 4. For the -30° inlet guide vane angle setting at *OL2*, the calculation in this particular case over-predicted the stress level by a factor of about 2. Therefore, a simple correction of the offset between the *FSI* calculation and the experiment can not be performed.

To demonstrate the influence of the inlet boundary condition for the time-resolved *CFD* calculation the inlet guide vanes were integrated into the *CFD* model. The comparison of the resulting unsteady blade pressure distribution with the case where the inlet boundary condition was taken from aerodynamic probe measurements downstream of the *IGV* row showed a significant reduction of the excitation amplitudes. The calculated blade stress was therefore under-predicted by more than one order of magnitude in the forced response calculation. It is therefore crucial to perform aerodynamic probe measurements of the distorted inlet flow field as close as possible to the impeller eye to increase the reliability of the numerical predictions.

It is evident that the use of measured inlet boundary conditions for the unsteady *CFD* calculation and experimentally estimated blade damping properties as input data for the forced response *FEM* calculation increase the fidelity of the predicted numerical stress level. However, a reliable prediction of the vibratory stress levels within the centrifugal impeller blades for the specific case presented in this paper necessitates additional effort to narrow the gap between the numerical prediction and the experiment.

ACKNOWLEDGEMENTS

The authors gratefully acknowledge the intellectual and financial support of their industrial partners ABB Turbo Systems Ltd. and MAN Diesel & Turbo Schweiz AG in this project. The substantial contributions of Dr. Janpeter Kuehnel, Dr. Francesco Colombo and Mr. Hans-Peter Dickmann from ABB Turbo Systems Ltd. and Dr. Beat Ribi and Mr. Yves Bidaut from MAN

Diesel & Turbo Schweiz AG are acknowledged. The authors would like to thank ABB Turbo Systems Ltd. for permission to publish this work. The experimental work and the unsteady *CFD* calculations were conducted at ETH Zurich. The fluid structure interaction calculations were performed at ABB Turbo Systems Ltd. The authors also acknowledge the financial support provided by the Swiss Confederation's innovation promotion agency, CTI.

REFERENCES

- [1] Srinivasan, A. V., 1997. "Flutter and resonant vibration characteristics of engine blades". *Journal of Turbomachinery-Transactions of the ASME*, **119**, pp. 741–775.
- [2] O'Brien, W. F., Cousins, W. T., and Sexton, M. R., 1980. *Unsteady pressure measurements and data analysis techniques in axial flow compressors*. ASME Book 100130.
- [3] Lakshminarayana, B., 1981. "Techniques for aerodynamic and turbulence measurements in turbomachinery rotors". *ASME Journal of Engineering for Gas Turbines and Power*, **103**, pp. 374–392.
- [4] Chivers, J. W. H., 1981. "Blade pressure measurements". In VKI Lecture Series 1981-7, Vol. Measurement Techniques in Turbomachines, VKI.
- [5] Dunn, M. G., Martin, H. L., and Stanek, M. J., 1986. "Heat-flux and pressure measurements and comparison with prediction for a low aspect ratio turbine stage". *Journal of Turbomachinery*, **108**, pp. 108–115.
- [6] Dunn, M. G., 1990. "Phase and time-resolved measurements of unsteady heat transfer and pressure in a full-stage rotating turbine". *Journal of Turbomachinery*, **112**, pp. 531–538.
- [7] Dunn, M. G., Bennett, W. A., Delaney, R. A., and Rao, K. V., 1992. "Investigation of unsteady flow through a transonic turbine stage: Data/prediction comparison for time-averaged and phase-resolved pressure data". *Journal of Turbomachinery*, **114**(1), pp. 91–99.
- [8] Rao, K. V., Delaney, R. A., and Dunn, M. G., 1994. "Vane-blade interaction in a transonic turbine, Part I: Aerodynamics". *Journal of Propulsion and Power*, **10**(3), pp. 305–311.
- [9] Dunn, M. G., 2001. "Convective heat transfer and aerodynamics in axial flow turbines". In ASME Gas Turbine Conference and Exhibit, Vol. 2001-GT-0506.
- [10] Miller, R. J., Moss, R. W., Ainsworth, R. W., and Harvey, N. W., 2003. "Wake, shock, and potential field interactions in a 1.5 stage turbine—Part I: Vane-rotor and rotor-vane interaction". *Journal of Turbomachinery*, **125**(1), pp. 33–39.
- [11] Miller, R. J., Moss, R. W., Ainsworth, R. W., and Harvey, N. W., 2003. "Wake, shock, and potential field interactions in a 1.5 stage turbine—Part II: Vane-vane interaction and

- discussion of results”. *Journal of Turbomachinery*, **125**(1), pp. 40–47.
- [12] Dénos, R., Sieverding, C., Arts, T., Brouckaert, J., Paniagua, G., and Michelassi, V., 1999. “Experimental investigation of the unsteady rotor aerodynamics of a transonic turbine stage”. *Proceedings of the Institution of Mechanical Engineers, Part A: Journal of Power and Energy*, **213**(4), pp. 327–338.
- [13] Dénos, R., Arts, T., Paniagua, G., Michelassi, V., and Martelli, F., 2001. “Investigation of the unsteady rotor aerodynamics in a transonic turbine stage”. *Journal of Turbomachinery*, **123**(1), pp. 81–89.
- [14] Manwaring, S. R., and Fleeter, S., 1990. “Inlet distortion generated periodic aerodynamic rotor response”. *Journal of Turbomachinery-Transactions of the ASME*, **112**(2), pp. 298–307.
- [15] Manwaring, S. R., and Fleeter, S., 1991. “Forcing function effects on rotor periodic aerodynamic response”. *Journal of Turbomachinery-Transactions of the ASME*, **113**(2), pp. 312–319.
- [16] Rabe, D. C., Bolcs, A., and Russler, P., 1995. “Influence of inlet distortion on transonic compressor blade loading”. In AIAA/ASME/SAE/ASEE Joint Propulsion Conference and Exhibit, 31st, Vol. AIAA 95-2461.
- [17] Miyakozawa, T., Kielb, R. E., and Hall, K. C., 2009. “The effects of aerodynamic asymmetric perturbations on forced response of blades disks”. *Journal of Turbomachinery - Transactions of the ASME*, **131**(4).
- [18] Kammerer, A., and Abhari, R. S., 2010. “Blade forcing function and aerodynamic work measurements in a high speed centrifugal compressor with inlet distortion”. *Journal of Engineering for Gas Turbines and Power - Transactions of the ASME*, **132**(9).
- [19] Filsinger, D., Szwedowicz, J., and Schaefer, O., 2002. “Approach to unidirectional coupled cfd-fem analysis of axial turbocharger blades”. *Journal of Turbomachinery*, **124**(1), pp. 125–131.
- [20] Filsinger, D., Frank, C., and Schaefer, O., 2005. “Practical use of unsteady cfd and fem forced response calculation in the design of axial turbocharger turbines”. *Proceedings ASME Turbo Expo*, pp. 601–612.
- [21] Dickmann, H. P., Wimmel, T. S., Szwedowicz, J., Filsinger, D., and Roduner, C. H., 2006. “Unsteady flow in a turbocharger centrifugal compressor: Three-dimensional computational fluid dynamics simulation and numerical and experimental analysis of impeller blade vibration”. *Journal of Turbomachinery-Transactions of the ASME*, **128**(3), pp. 455–465.
- [22] Zemp, A., Ribí, B., and Abhari, R. S., 2011. “Experimental investigation of forced response impeller blade vibration in a centrifugal compressor with variable igvs – part 1: blade damping”. In ASME Turbo Expo, Vol. GT2011–46289.
- [23] Schleer, M., 2006. *Flow structure and stability of a turbocharger centrifugal compressor*. Dissertation ETH Nr. 16605. VDI-Verlag, Düsseldorf.
- [24] Lenherr, C., Kalfas, A., and Abhari, R. S., 2011. “High temperature fast response aerodynamic probe”. *Journal of Engineering for Gas Turbines and Power*, **133**(1).
- [25] Gossweiler, C. R., 1993. *Sonden und Messsystem für schnelle aerodynamische Strömungsmessung mit piezoresistiven Druckgebern*. Diss. ETH Nr. 10253. Zürich.
- [26] Kupferschmied, P., 1998. *Zur Methodik zeitaufgelöster Messungen mit Strömungs sonden in Verdichtern und Turbinen*. Diss. ETH Nr. 12474. Zürich.
- [27] Pfau, A., Schlienger, J., Kalfas, A. I., and Abhari, R. S., 2003. “Unsteady, 3-dimensional flow measurement using a miniature virtual 4 sensor fast response aerodynamic probe (FRAP)”. In ASME Turbo Expo, Vol. GT2003–38128.
- [28] Kammerer, A., 2010. *Experimental research into resonant vibration of centrifugal compressor blades*. ETH Dissertation No. 18587. Zurich.
- [29] Zemp, A., Kammerer, A., and Abhari, R. S., 2010. “Unsteady computational fluid dynamics investigations on inlet distortion in a centrifugal compressor”. *Journal of Turbomachinery - Transactions of the ASME*, **132**(3).
- [30] Schmitz, M. B., Schaefer, O., Szwedowicz, J., Wimmel, T. S., and Sommer, T. P. “Axial turbine blade vibrations by stator flow - comparison of calculations and experiment”. *ISUAAAT*.
- [31] Dickmann, H. P., Wimmel, T. S., Szwedowicz, J., Kuehnel, J., and Essig, U., 2009. “Unsteady flow in a turbocharger centrifugal compressor: 3D-CFD simulation, impeller blade vibration and vaned diffuser-volute interaction”. In Proceedings of ASME Turbo Expo 2009, Vol. GT2009-59046.